Tungsten Promotes Sex-Specific Adipogenesis in the Bone by Altering Differentiation of Bone Marrow-Resident Mesenchymal Stromal Cells

Alicia M. Bolt,[*,†] Michael P. Grant,[*] Ting Hua Wu,[*,‡] Manuel Flores Molina,[*] Dany Plourde,[*] Alexander D. R. Kelly,[*,§] Luis Fernando Negro Silva,[*,‡] Maryse Lemaire,[*,†] Jennifer J. Schlezinger,[‖] Fackson Mwale,[*,§,¶] and Koren K. Mann[*,†,‡,1]

[*]Lady Davis Institute for Medical Research; [†]Department of Oncology; [‡]Division of Experimental Medicine; [§]Faculty of Medicine; [¶]Department of Surgery, McGill University, Montréal, Québec, Canada; and [‖]Department of Environmental Health, Boston University School of Public Health, Boston, Massachusetts, USA

[1]To whom correspondence should be addressed at Lady Davis Institute for Medical Research, 3755 Côte Ste Catherine Rd, Rm E537, Montréal, Québec, H3T 1E2, Canada. E-mail: koren.mann@mcgill.ca.

ABSTRACT

Tungsten is a naturally occurring metal that increasingly is being incorporated into industrial goods and medical devices, and is recognized as an emerging contaminant. Tungsten preferentially and rapidly accumulates in murine bone in a concentration-dependent manner; however the effect of tungsten deposition on bone biology is unknown. Other metals alter bone homeostasis by targeting bone marrow-derived mesenchymal stromal cell (MSC) differentiation, thus, we investigated the effects of tungsten on MSCs *in vitro* and *in vivo*. *In vitro*, tungsten shifted the balance of MSC differentiation by enhancing rosiglitazone-induced adipogenesis, which correlated with an increase in adipocyte content in the bone of tungsten-exposed, young, male mice. Conversely, tungsten inhibited osteogenesis of MSCs *in vitro*; however, we found no evidence that tungsten inhibited osteogenesis *in vivo*. Interestingly, two factors known to influence adipogenesis are sex and age of mice. Both female and older mice have enhanced adipogenesis. We extended our study and exposed young female and adult (9-month) male and female mice to tungsten for 4 weeks. Although tungsten accumulated to a similar extent in young female mice, it did not promote adipogenesis. Interestingly, tungsten did not accumulate in the bone of older mice; it was undetectable in adult male mice, and just above the limit of detect in adult female mice. Surprisingly, tungsten enhanced adipogenesis in adult female mice. In summary, we found that tungsten alters bone homeostasis by altering differentiation of MSCs, which could have significant implications for bone quality, but is highly dependent upon sex and age.

Key words: tungsten; bone; mesenchymal stromal cell; osteogenesis; adipogenesis; metals.

Tungsten is used in manufacturing, particularly in alloys, because of the properties it imparts: flexibility, strength, and conductance. Extensive use of tungsten has increased exposure occupationally and environmentally (NIOSH, 1977; Rubin *et al.*, 2007; Tyrrell *et al.*, 2013). Recently, the Environmental Protection Agency (EPA) classified tungsten as an emerging contaminant that warrants further toxicological investigation (EPA, 2008), which highlights the

importance of defining the toxicological profile and long-term human health effects of tungsten. In addition, tungsten has been incorporated into implanted medical devices (e.g. drug-eluting stents, embolism coils, radiotherapy shields), identifying a new population that is potentially at risk for high level tungsten exposure (Bachthaler *et al.*, 2004; Bolt *et al.*, 2015). We recently described a cohort of breast cancer patients, who were left with residual

tungsten in their breasts during a clinical trial testing a tungsten-based shield used during intraoperative radiotherapy (Bolt et al., 2015). Tungsten was measured in the blood and urine of these women several years following initial exposure, indicating that tungsten is mobilized and distributed throughout the body. Importantly, tungsten was still found in women who had opted for mastectomy to remove breast-resident tungsten, suggesting that there is a storage reservoir for tungsten in humans. In spite of the rise in the number of individuals exposed to high levels of tungsten, there is a lack of knowledge of the potential toxicological effects of tungsten and the long-term human health risks.

Tungsten accumulates preferentially in murine bone (Guandalini et al., 2011). In addition, tungsten accumulates faster than it is removed from the bone following cessation of exposure (Kelly et al., 2013). Furthermore, standard chelation therapy that is used to remove other metals, such as lead or copper from the body, cannot mobilize tungsten in humans (Bolt et al., 2015). Thus, exposure to tungsten can result in persistent endogenous exposure. Although it is known that tungsten accumulates in bone, the consequences of tungsten exposure on bone biology are unknown.

Several other metals are known to alter bone homeostasis. Lifetime lead exposure results in an osteoporotic phenotype and an increase in adipogenesis in the bone marrow cavity of rats (Beier et al., 2013). The lead-induced osteoporotic phenotype likely results from an alteration in the balance of osteoblast and adipocyte differentiation of bone marrow-resident mesenchymal stromal cells (MSCs). MSCs are the precursor stem cells to multiple lineages, including osteoblasts, adipocytes, chondrocytes, and myoblasts. Lead inhibits osteogenesis and induces adiopogenesis of MSCs, leading to changes in bone architecture (Beier et al., 2013). Organotins, commonly found in pesticides and plastics manufacturing, induce Peroxisome Proliferation-Acitvated Receptor Gamma (PPARγ)-dependent adipocyte differentiation of MSCs (Yanik et al., 2011). Arsenic suppresses osteoblast differentiation of rat-derived MSCs *in vitro*, which is associated with a decrease in bone mineral density and microstructure (Wu et al., 2014). Conversely, arsenic has been shown to suppress adipogenesis and promote osteogenesis of MSCs derived from humans (Cheng et al., 2011; Klei et al., 2013). Thus, the MSC is a key target cell whose differentiation can be altered by metals and may have profound effects on bone health.

Here, we investigated the effects of tungsten on bone using *in vitro* and *in vivo* models and show that tungsten promotes adipogenesis in mice; however, this response is dependent on sex and age. Furthermore, we find that tungsten promotes adipogenesis induced by the PPARγ ligand rosiglitazone, although tungsten does not activate PPARγ itself. Conversely, tungsten inhibits osteogenesis of MSCs. Together, our data indicate that tungsten can alter bone homeostasis, and thus could have profound effects on bone health long term.

MATERIALS AND METHODS

In Vivo Exposure

All animal experiments were approved by the McGill University Animal Care Committee (Montréal, Quebec, Canada). Wild-type C57BL/6 mice (male and female, 4-weeks old; male and female, 9-months old) were purchased from either Jackson Laboratory (Bar Harbor, Massachusetts) or Charles Rivers Laboratories Inc. (Montréal, Quebec, Canada) and housed in the Lady Davis Institute Animal Care Facility. Mice were given food and water *ad libitum*. For *in vivo* tungsten exposures, mice were divided into 2 groups: control tap water or 15 parts per million (ppm; μg/ml) tungsten (sodium tungstate). Sodium tungstate dihydrate ($Na_2WO_4 \cdot 2H_2O$; Sigma-Aldrich, St Louis, Missouri) was dissolved in tap water and replaced every 2 or 3 days to limit conversion to polytungstates (Kelly et al., 2013). The concentration of tungsten used in our study represents elemental tungsten as opposed to the dihydrate compound (1.795 g $Na_2WO_4 \cdot 2H_2O$ = 1 g tungsten). After 1 week of acclimatization, mice were exposed to tap water or tungsten in drinking water for 4 weeks. Young mice were 5-weeks old and adult (middle-aged) mice were 9-months old at the start of the exposure. We observed no differences in the levels of tungsten deposition in the bone in C57BL/6 mice of comparable age purchased from either source. As we have previously published (Kelly et al., 2013), no changes in animal weight, physical appearance, or water intake were observed in the tungsten-exposed group. After the 4-week exposure, mice were euthanized by CO_2 asphyxiation followed by terminal cardiac puncture. Femur bones were dissected and fixed intact in Accustain (Sigma-Aldrich, St Louis, Missouri). Humeri bones were dissected, flushed to remove bone marrow, and frozen at −20°C to use for tungsten concentration analysis. Tibiae bones were dissected and fixed intact in 70% ethanol and stored at −80°C. An additional set of male mice (5 weeks) was given tap water or water containing 15 ppm tungsten for 4 weeks. At the end of the exposure, mice were euthanized and total bone marrow was flushed from femurs, tibiae, and humeri and used to analyze expression of osteoblast and adipocyte gene markers.

Tungsten Analysis

Tungsten concentration in humeri bones was quantified by Inductively Coupled Plasma Mass Spectrometry (ICP-MS), as previously described in Bolt et al. (2015) and Kelly et al. (2013). Data were reported as mean tungsten concentration (ppm) per weight of bone ± SEM, $n \geq 4$. The elemental limit of detection was set to 0.5 ppm.

Perilipin Immunohistochemistry (IHC)

Femur bones, harvested from mice exposed *in vivo* and fixed in Accustain, were decalcified in hydrochloric acid and formic acid solution, paraffin embedded, and sectioned. Slides were incubated with anti-perilipin antibody (1:100, Cell Signaling no. 9349S, Danvers, Massachusetts) at 4°C overnight, followed by biotinylated anti-rabbit secondary antibody at room temperature for 30 min. Slides were processed using the peroxidase VECTASTAIN ABC kit (Vector Laboratories, Burlingame, California), and developed with ImmPACT DAB peroxidase substrate (Vector Laboratories, Burlingame, California). Sections were counterstained with 20% Harris-modified hematoxylin (Thermo Fisher Scientific, Waltham, Massachusetts) and mounted in Permount (Thermo Fisher Scientific, Waltham, Massachusetts). Slides were scanned using an Aperio Scanscope AT Turbo scanner (Leica Biosystems, Concord, Ontorio, Canada). The number and size of perilipin-positive (perilipin[+]) adipocytes within the entire bone marrow cavity of each femur tissue section was analyzed using Aperio ScanScope software (Leica Biosystems, Concord, Ontario, Canada). The adipocytes were identified on scans of an entire bone section and the circumference manually drawn to determine the area using the Aperio software (data reported as area, μm^2). Data were reported as the total number of perilipin[+] adipocytes per animal, the average size of perilipin[+] adipocytes per animal, and the total area of bone marrow occupied by perilipin[+] adipocytes per

animal. One control sample from the young male mice and one tungsten sample from the adult female mice analysis were excluded because they were determined to be outlying data points using the Grubb's test for outliers statistical test ($P \leq .05$).

Alkaline Phosphatase Activity Histology Staining

Tibiae bones, harvested from mice exposed *in vivo* (young males, 5-weeks old), were fixed in 70% ethanol and stored at $-80°C$ until embedding. Fixed, undecalcified bones were embedded in methylmethacrylate and sectioned. To assess alkaline phosphatase (ALP) enzymatic activity, sections were stained using the Vector Red Alkaline Phosphatase Substrate Kit (Vector Labs, Burlingame, California) according to manufacturer's protocol. Sections were counter-stained with methyl green. Staining was performed at the McGill Bone Center (McGill University, Montreal Quebec, Canada). Images ($20\times$) were taken of cortical and trabecular bone regions. Images were analyzed using Aperio ScanScope software (Leica Biosystems, Concord, Ontario, Canada). Data were reported as the average alkaline phosphate thickness and the number of positive pixels per area. ALP thickness was quantified using the color deconvolution v9 algorithm. Thickness (μm) was calculated by dividing the total positive area (μm^2) by the length of the region analyzed. The number of positive pixels per area was quantified using the positive pixel count v9 algorithm. The number of positive pixels was calculated by taking the sum of all the positive pixels and divided by the total area of each region analyzed. If more than one region was analyzed per image, the values were averaged together and one value was recorded per image.

MSC Primary Cultures

Primary bone marrow-derived stromal cell cultures were prepared from untreated, wild-type C57BL/6 mice (male, 9–12 weeks of age). Bone marrow was flushed from the femurs, tibiae, and humeri and strained through a 70-μm cell strainer to remove any tissue debris. Cells were cultured in MSC medium consisting of α-MEM medium (Wisent, St Bruno, Quebec, Canada) supplemented with 10% FBS (Wisent, St Bruno, Quebec, Canada), 100 U/ml penicillin, 100 μg/ml streptomycin, and 0.25 μg/ml amphotericin B (MP Biomedicals, Solon, Ohio). Cells were plated as follows in order to maintain the same cell confluence per experiment: 96-well plate (75 000 cells per well), 24-well (3×10^6 per well), 12-well plate (6×10^6 per well), and 6-well plate (12×10^6 per well). After 7 days, naïve cells were harvested to use as undifferentiated controls. The remaining cell cultures were then differentiated into either osteoblasts or adipocytes. MSC cultures, following the initial 7-day culture, were differentiated into osteoblasts by culture in OM medium (MSC medium supplemented with 10 nM dexamethasone, 12.5 μg/ml L-ascorbic acid, 8 mM β-glycerol phosphate, and 0.5 μg/ml insulin). MSC cultures, following the initial 7-day culture, were differentiated into adipocytes by culture in OM medium and treated with or without 1 nM rosiglitazone. Both osteogenic or adipogenic cultures were evaluated untreated or treated with 15 μg/ml sodium tungstate dihydrate throughout the differentiation process. Cultures were differentiated in OM medium plus treatments for 7–12 days depending on the experimental protocol. For *ex vivo* experiments, bone marrow was flushed from male mice (5 weeks) exposed, *in vivo*, to tap water or 15 ppm tungstate for 4 weeks. Bone marrow was pooled from 4 animals per exposure group to set up *ex vivo* MSC cultures. *Ex vivo* cultures were differentiated in OM medium with or without treatment of 1 nM rosiglitzone for 7–12 days depending on the experimental protocol.

Caspase 3/7 Assay

Apoptotic cell death was assessed by measuring caspase 3/7 activity, using the Caspase-Glo 3/7 Kit (Promega, Madison, Wisconsin), according to manufacturer's protocol. Briefly, MSCs were isolated as described previously and seeded in a 96-well white-walled plate. MSCs were allowed to adhere and grow for 7 days in MSC medium. At day 7, cell media was changed to OM medium to start the differentiation process and cells were left untreated or treated with 100 nM rosiglitazone, 15 μg/ml sodium tungstate dihydrate, or the combination for 10 days. As a positive control, cells maintained in OM media were treated with 0.25 μM staurosporine for 18 h. At day 10 of differentiation, cell lysis buffer containing caspase 3/7 substrate was added to each well (equal volumes of media and lysis buffer) and luminescence was read using a Fluostar Optima microplate reader (BMG Labtech, Ortenberg, Germany). Background luminescence was subtracted from each well. Data were reported as mean luminescence $\pm$ SEM for each group.

Quantitative Reverse Transcriptase PCR Gene Expression Analysis

Total RNA was isolated from MSC cultures or from total bone marrow harvested from mice exposed *in vivo* by Trizol extraction (Life Technologies, Grand Island, New York). cDNA was prepared from total RNA using the iScript cDNA synthesis kit (Biorad, Mississauga, Ontario, Canada). Gene expression was analyzed by **quantitative reverse transcriptase** (qRT)-PCR using the Applied Biosystems 7500 Fast RT-PCR system, using Fast SYBR Green Master Mix (Life Technologies, Grand Island, New York). Experiments were performed using validated qRT-PCR primers purchased from Qiagen (Toronto, Ontario, Canada): *Rn18s* (QT02448075), *Pparg* (QT00100296), *Fabp4* (QT00091532), *Plin1* (QT00150360), *Runx2* (QT00102193), *Bglap* (Osteocalcin) (QT00259406), and *Sp7* (Osterix) (QT00293181), or designed and purchased from Integrated DNA Technologies (Coralville, Iowa): *Adipoq*, *Gapdh*, and *m36B4*. Primer sequences are available for designed primers in Supplementary Table 1. For the *in vitro* MSC cultures, adipocyte marker gene expression was analyzed at day 7 of differentiation and the osteoblast marker gene expression was analyzed at day 10 of differentiation. For each sample qRT-PCR was performed in 4 technical replicates. For the *in vitro* MSC samples, data were normalized to the housekeeping gene *Rn18s*. Fold change in gene expression was determined by the $2^{-\Delta\Delta Ct}$ method using the expression of undifferentiated cells (naïve) as the reference. For the total bone marrow *in vivo* samples, data were normalized to the housekeeping genes *Gapdh* and *m36B4*. Fold change in gene expression was determined by the $2^{-\Delta\Delta Ct}$ method using the expression of one control bone marrow sample as the reference.

Phenotype Assays

Oil red O staining

Lipid accumulation was visualized by Oil Red O staining at day 9 of differentiation. MSC cells were cultured in 24-well black-walled tissue cultures plates. At day 9 of differentiation, cells were fixed in 2% paraformaldehyde and stained with Oil Red O (Electron Microscopy Sciences, Hatfield, Pennsylvania) for 1 h at room temperature. Samples were washed with $1\times$ PBS and

counterstained with 1:10 dilution of hematoxylin and imaged (10×).

Adipocyte quantification

The number of adipocytes per well in the MSC cultures at day 9 of differentiation was calculated by the sum of the number of adipocytes from 3 representative images (10×) of Oil Red O stained cells. The data were expressed as the mean number of adipocytes per well ± SEM for each group.

ALP activity

ALP activity was assessed at day 12 of differentiation. MSC cells were cultured in 12-well plates, fixed with 2% paraformaldehyde, and incubated with p-nitrophenyl phosphate solution (Sigma-Aldrich, St Louis, Missouri). The reaction was stopped by adding NaOH. Absorbance was measured at 405 nm in 96-well white-walled plates using the Benchmark Plus plate reader (Bio-rad, Mississauga, Ontario Canada). Data were represented as the mean ALP absorbance ± SEM for each group.

Alizarin Red staining

Following analysis of ALP, cells were stained with Alizarin Red (Osteogenesis Quantitation Kit, Millipore, Billerica, Massachusetts) to evaluate calcium mineralization. Following staining, cells were extensively washed and imaged. Alizarin Red was quantified according to manufacturer's protocol by measuring absorbance at 405 nm in 96-well white-walled plates using the Benchmark Plus plate reader (Bio-rad, Mississauga, Ontario, Canada). Before reading absorbance, some samples were diluted in H_2O to have the absorbance be within the detection range of the plate reader. If one sample for a particular experiment needed to be diluted then all the samples for that experiment were diluted to the same dilution factor to have comparable absorbance values. Data were represented as the mean Alizarin Red absorbance ± SEM for each group.

PPARγ Reporter Assay

Cos-1 cells were maintained in DMEM media (Wisent, St. Bruno, Quebec, Canada) supplemented with 10% FBS (Wisent, St Bruno, Quebec, Canada) and 1% penicillin-streptomycin (Wisent, St Bruno, Quebec, Canada). Cos-1 cells (150 000) were seeded in 12-well plates. Cells were co-transfected with equal concentrations of pcDNA3-FLAG-hPPARγ receptor (gift from V.K.K. Chatterjee, University of Cambridge), *Renilla* reporter and PPAR response-element driven luciferase reporter (PPRE-Luc; Mann et al., 2005) plasmids (0.625 μg) in a 3:2 ratio of Lipofectamine 2000 (Invitrogen, Burlington, Ontario, Canada) to total DNA. After 4 h, cells were either left untreated or treated with either 100 nM rosiglitazone or 15 μg/ml sodium tungstate dihydrate. Twenty-four hours post transfection, cells were lysed and luminescence was measured using the Dual-Luciferase Reporter Assay (Promega, Madison Wisconsin) following manufactures protocol. Luminescence was measured using the Glomax 20/20 Luminometer (Promega, Madison Wisconsin). The level of PPRE-Luc luminescence activity was normalized to the level of *Renilla* luminescence activity of each well.

Statistics

All statistics were performed using GraphPad Prism version 4 software (GraphPad, La Jolla, California). For comparisons between 2 groups, an unpaired student t test analysis was performed. For comparisons between 3 or more groups, a 1-way ANOVA analysis was performed followed by Bonferroni *post hoc* tests. For the *in vivo* adipocyte characterization, comparisons were made between control and tungsten expose samples for each group (young male, young female, adult male, and adult female) by unpaired, 1-tailed student t tests.

RESULTS

Tungsten Does Not Activate PPARγ Alone, but Acts to Enhance Rosiglitazone-Induced Adipogenesis of MSCs *In Vitro*

Bone marrow-resident MSCs are an important cellular component in the bone marrow. Other metals, such as lead and organotins, affect bone biology by altering MSC differentiation into adipocytes (Beier et al., 2013; Yanik et al., 2011). In order to evaluate the effect of tungsten on MSC differentiation into adipocytes, we utilized a primary mouse MSC culture system that can be differentiated into either osteoblasts or adipocytes. MSCs were cultured in OM media and exposed to 15 μg/ml tungsten, 1 nM rosiglitazone, or the combination throughout adipocyte differentiation. No standard has been defined for tungsten in the drinking water; the only established action levels are in the State of Massachusetts, United States: 1–2 ppm in soil and 15 ppm in groundwater (EPA, 2012). In our previous studies, 15 ppm is the concentration at which we observed tungsten-induced changes in mice (Bolt et al., 2015; Kelly et al., 2013). Thus, a concentration of 15 μg/ml (equivalent to ppm) tungsten was chosen for the *in vitro* treatments. We measured expression of adipocyte gene markers by qRT-PCR. PPARγ (*Pparg*) is the master regulator of adipocyte differentiation. *Fabp4* is a PPARγ target gene and is a carrier protein for fatty acids (Tontonoz et al., 1994). *Adipoq* is a PPARγ target gene for the adipocyte specific hormone adiponectin (Park et al., 2004). Perilipin (*Plin1*) regulates lipolysis in mature adipocytes (Greenberg et al., 1991). At day 7 of differentiation, tungsten alone did not increase the mRNA expression of adipocyte markers *Pparg*, *Fabp4*, *Plin1*, or *Adipoq* (Figure 1A). However, tungsten enhanced the rosiglitazone-induced increase in expression of the adipocyte markers (Figure 1A). Consistent with these results, tungsten also enhanced the number of adipocytes induced by rosiglitazone, as visualized and counted by Oil Red O staining at day 9 of differentiation (Figs. 1B and C).

Certain agents, such as rosiglitazone and organotins, promote adipogenesis by serving as ligands for PPARγ (Yanik et al., 2011). To evaluate the ability of tungsten to act as a ligand for PPARγ, we assessed activation of PPARγ transcriptional activity stimulated by tungsten in comparison to rosiglitazone (positive control) using a reporter assay. Unlike rosiglitazone, a potent, therapeutic PPARγ ligand and adipogenic agent (Gimble et al., 1996), tungsten did not stimulate PPARγ transcriptional activity (Supplemental Figure S1). These data suggest that tungsten, while not capable of inducing adipocyte differentiation alone, enhances rosiglitazone-induced adipogenesis of MSCs *in vitro*.

In Vivo, Tungsten Exposure Increases Adipocyte Number in Bone Marrow

In order to determine whether incorporation of tungsten into bone resulted in increased adipogenesis *in vivo*, we exposed 5-week old male mice to 15 ppm tungsten orally for 4 weeks. The mean humeri bone concentration of tungsten accumulated after the 4-week oral exposure was 5.7 ppm ± SEM 1.3), which is comparable to tungsten concentrations we have previously
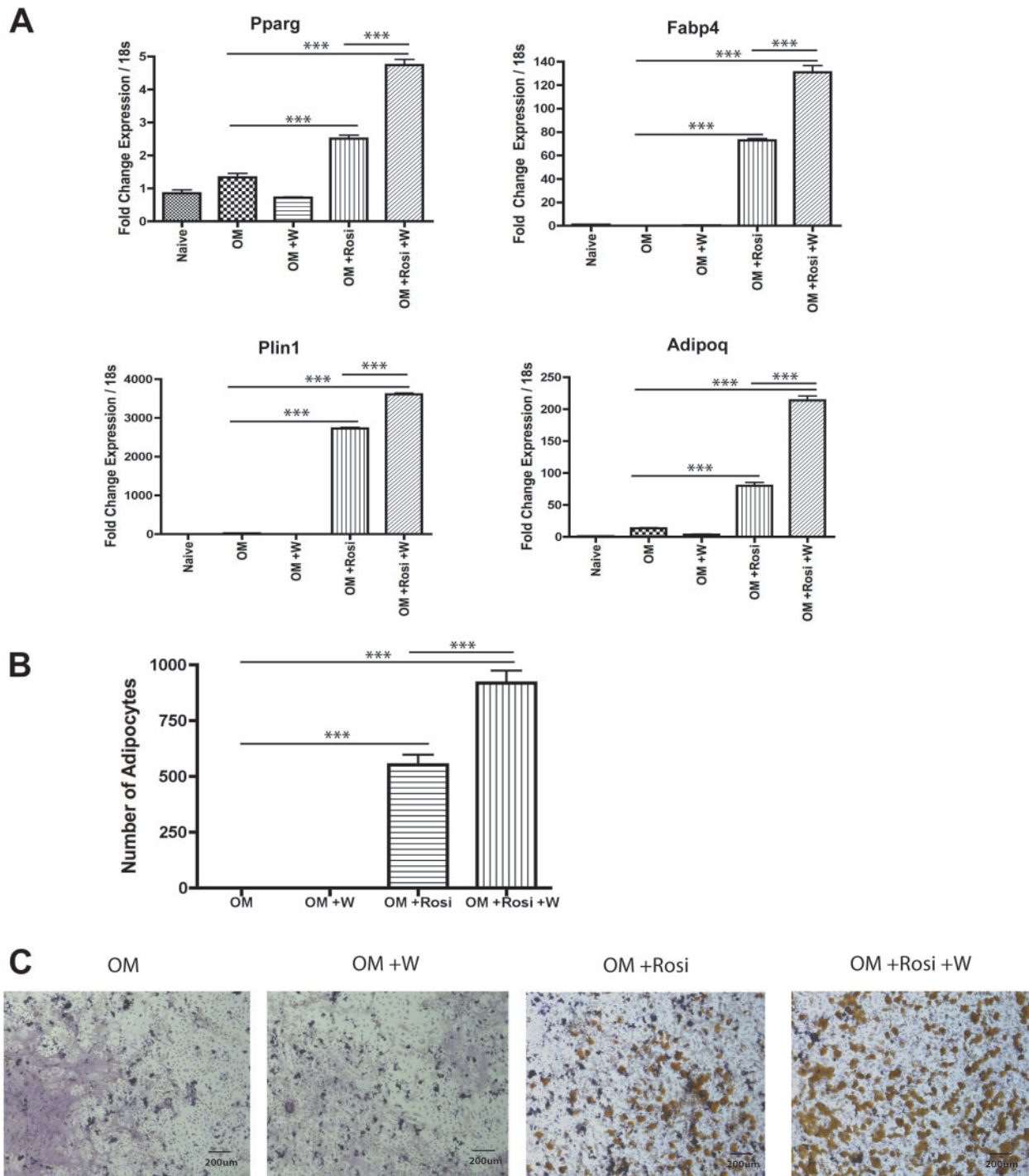
FIG. 1. Tungsten enhances rosiglitazone-induced adipogenesis of MSCs *in vitro*. MSC cultures were transitioned to OM medium and were either left untreated (OM) or treated with 15 μg/ml tungsten (OM +W), 1 nM rosiglitazone (OM +Rosi), or the combination of tungsten and rosiglitazone (OM +Rosi +W) throughout adipocyte differentiation. A, RNA expression analysis of adipocyte gene markers (*Pparg*, *Fabp4*, *Plin1*, and *Adipoq*) were analyzed by qRT-PCR at day 7 of differentiation. Graph shows the mean fold change in gene expression ± SEM, normalized to naïve gene expression for each gene. Data normalized to housekeeping gene *Rn18s*. ***$P \leq .001$ 1-way ANOVA. Graph is a representative experiment of 3 biological replicates each performed in four technical replicates. B, Adipocyte quantification in MSC cultures was analyzed by counting the number of adipocytes in 3 representative images (10×) of Oil Red O stained cells per sample at day 9 of differentiation. Graph shows the number of adipocytes ± SEM. Graph is a representative experiment of 3 biological replicates each performed in triplicate. ***$P \leq .001$ 1-way ANOVA. C, Representative images (10×) of Oil Red O stained MSC cultures at day 9 of differentiation.

measured in tibiae bones (5.9 ppm ± SEM 0.3; Kelly *et al.*, 2013). We measured adipocyte gene markers by qRT-PCR in total bone marrow harvested from mice exposed to tungsten *in vivo*. After the 4-week exposure, tungsten increased the mRNA expression levels of adipocyte markers *Pparg* and *Fabp4*; however, there was no significant change in *Adipoq* (Figure 2A; *Plin1* expression was below the limit of detection so data were not included).
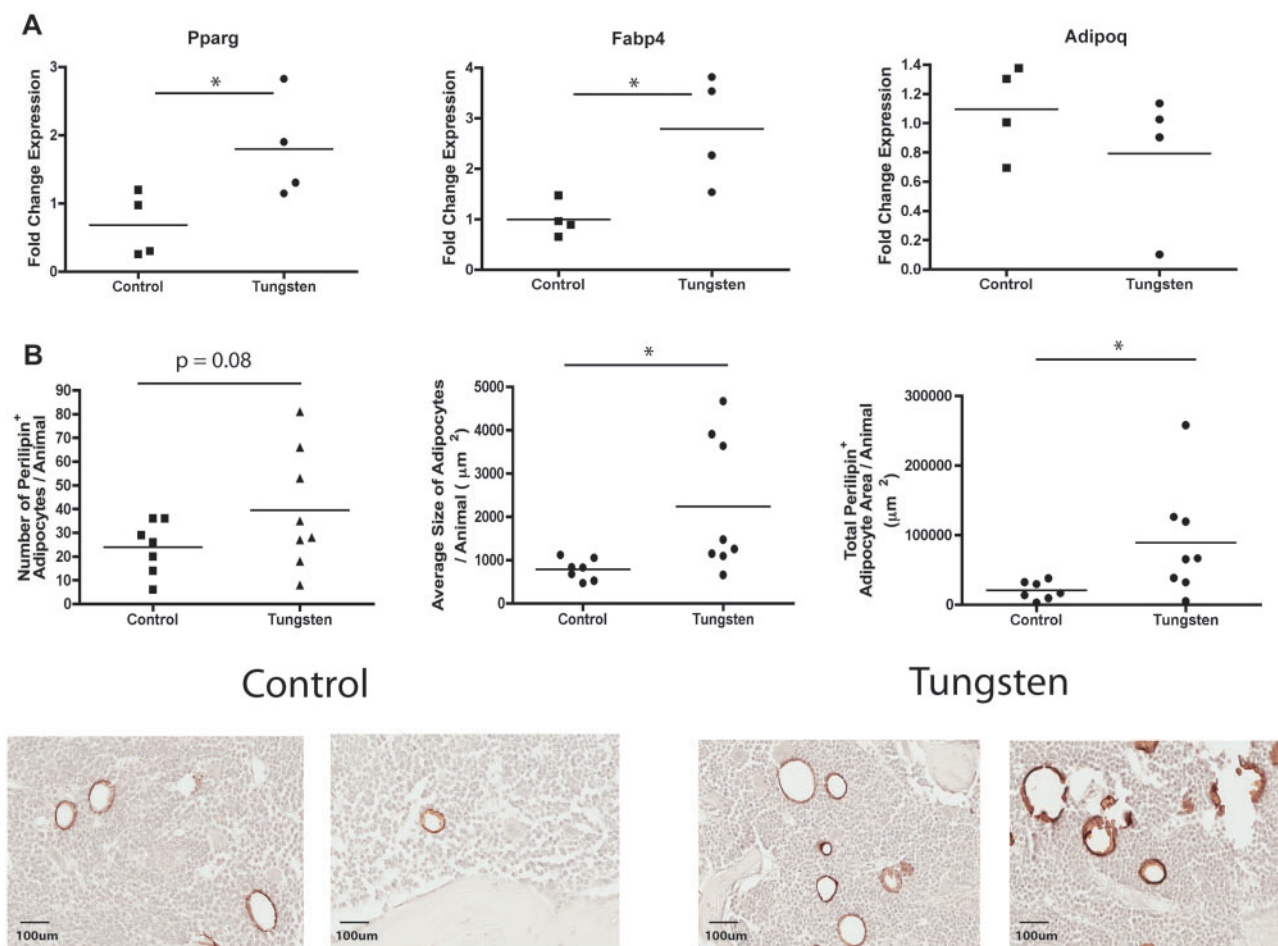
FIG. 2. Tungsten promotes adipogenesis in the bones of mice. Male C57BL/6 mice (5 weeks) were given tap water (control) or 15 ppm tungsten in drinking water for 4 weeks. **A,** RNA expression analysis of adipogenic gene markers *Pparg*, *Fabp4*, *Adipoq* in total bone marrow isolated from control and tungsten exposed animals, analyzed by qRT-PCR. Graph shows mean fold change in gene expression normalized to one control sample ($n = 4$). Data normalized to housekeeping genes *Gapdh* and *m36B4*. *$P \leq .5$ unpaired student t test, 2-tailed. **B,** Analysis of perilipin staining by IHC in sections of femur bone tissue from control and tungsten exposed animals. Graphs show the mean number of perilipin$^+$ adipocytes/animal, average size of each adipocyte/animal, and the total perilipin$^+$ adipocyte area/animal ($n \geq 7$). Representative images of perilipin$^+$ adipocytes in control and tungsten-exposed femur sections, 20×. *$P \leq .05$, unpaired student t-test, one-tailed. **C,** *Ex vivo* MSC cultures were derived from control and tungsten-exposed mice and differentiated in the absence of tungsten *in vitro*. Cultures were transitioned to osteoinductive medium and were either left untreated (Control OM or Tungsten OM) or treated with 1 nM rosiglitazone (Control OM + Rosi or Tungsten OM +Rosi) throughout adipocyte differentiation. RNA expression analysis of adipogcyte gene markers (*Pparg*, *Fabp4*, *Plin1*, and *Adipoq*) in *ex vivo* MSC cultures analyzed by qRT-PCR at day 7 of differentiation. Graph shows the mean fold change in gene expression ± SEM ($n = 3$), normalized to naïve gene expression for each gene. Table shows the mean fold change in gene expression ± SEM ($n = 3$) for Control and Tungsten samples cultured in OM media alone, normalized to naïve gene expression for each gene. Graphs **$P \leq .01$ 1-way ANOVA. Table *$P \leq .05$, **$P \leq .01$ unpaired student t test, 1-tailed. **D,** Adipocyte quantification in *ex vivo* MSC cultures was analyzed by counting the number of adipocytes in 3 representative images (10×) of Oil Red O stained cells per sample at day 9 of differentiation. Graph shows the number of adipocytes ± SEM ($n = 6$). *$P \leq .05$ 1-way ANOVA.

Because we observed an increase in the expression of the adipogenic markers, we further evaluated the effect of tungsten exposure on adipogenesis by staining femur bone sections for the adipocyte marker perilipin by immunohistochemistry (IHC). We observed an increase in the total number of perilipin$^+$ adipocytes in the tungsten-exposed animals (unpaired student t test, $P = .08$; Figure 2B). In the tungsten-exposed mice, the perilipin$^+$ adipocytes were significantly larger than adipocytes from control animals, which resulted in a greater total bone area occupied by adipocytes per animal (Figure 2B). Interestingly, the effect of tungsten on adipocyte size does not seem to be a uniform response. Two responses are evident: one that has slightly larger adipocyte size than control animals and a second group that has much larger adipocytes (Figure 2B). This could suggest that other confounding factors are affecting tungsten-enhanced adipogenesis.

Since we observed an increase in the expression of adipocyte genes and adipocyte content within the bone of exposed mice, we next determined whether *in vivo* tungsten exposure could pre-program MSCs to respond to PPAR ligands, resulting in enhanced adipogenesis *in vitro*. We cultured MSCs from mice exposed to tap water or water containing 15 ppm tungsten, *in vivo* for 4 weeks, and differentiated them into adipocytes *in vitro* with and without treatment of 1 nM rosiglitazone over the course of the differentiation protocol. At day 7 of differentiation, MSCs from tungsten-exposed animals cultured in OM media (Tungsten MSC) had elevated mRNA levels of all 4 adipocyte markers in comparison to MSCs from control mice cultured in OM media (Figure 2C). These data support our observations *in vivo* of increased mRNA expression of adipocyte specific markers *Pparg* and *Fabp4* in total bone marrow harvested from tungsten-exposed mice (Figure 2A). In addition, Tungsten MSC

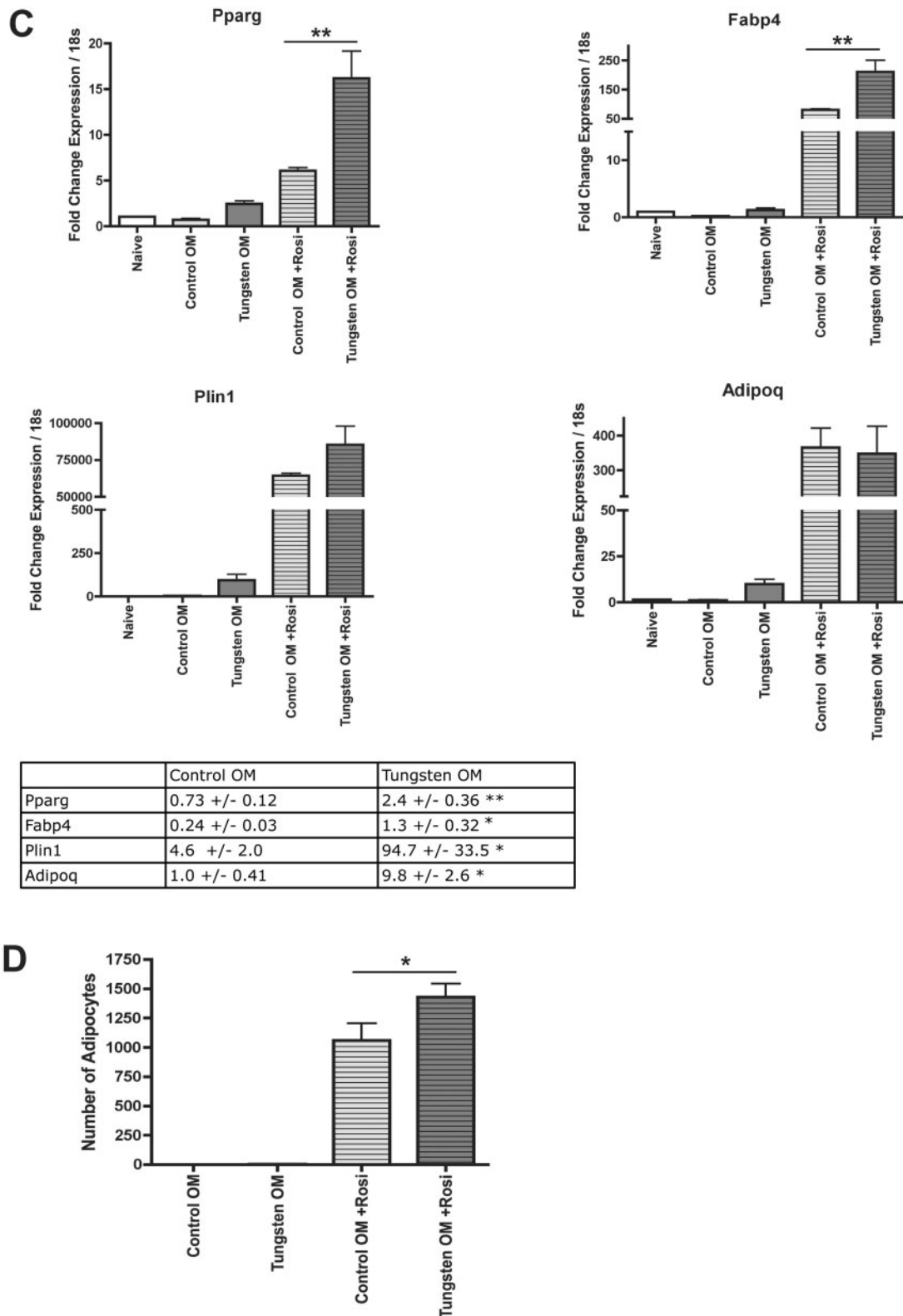|	Control OM	Tungsten OM
Pparg	0.73 +/- 0.12	2.4 +/- 0.36 **
Fabp4	0.24 +/- 0.03	1.3 +/- 0.32 *
Plin1	4.6 +/- 2.0	94.7 +/- 33.5 *
Adipoq	1.0 +/- 0.41	9.8 +/- 2.6 *

FIG. 2. Continued.

cultures treated with rosiglitazone had enhanced mRNA expression of adipocyte specific markers *Pparg*, *Fabp4* and *Plin1*, but only *Pparg* and *Fabp4* were statistically significant (Figure 2C; 1-way ANOVA, $P \leq .05$) when compared with rosiglitazone-treated MSC cultures generated from control mice. Phenotypically, Tungsten MSCs cultured in OM media did not have visible adipocytes when quantified by oil red O staining, even though they had an increase in mRNA expression of
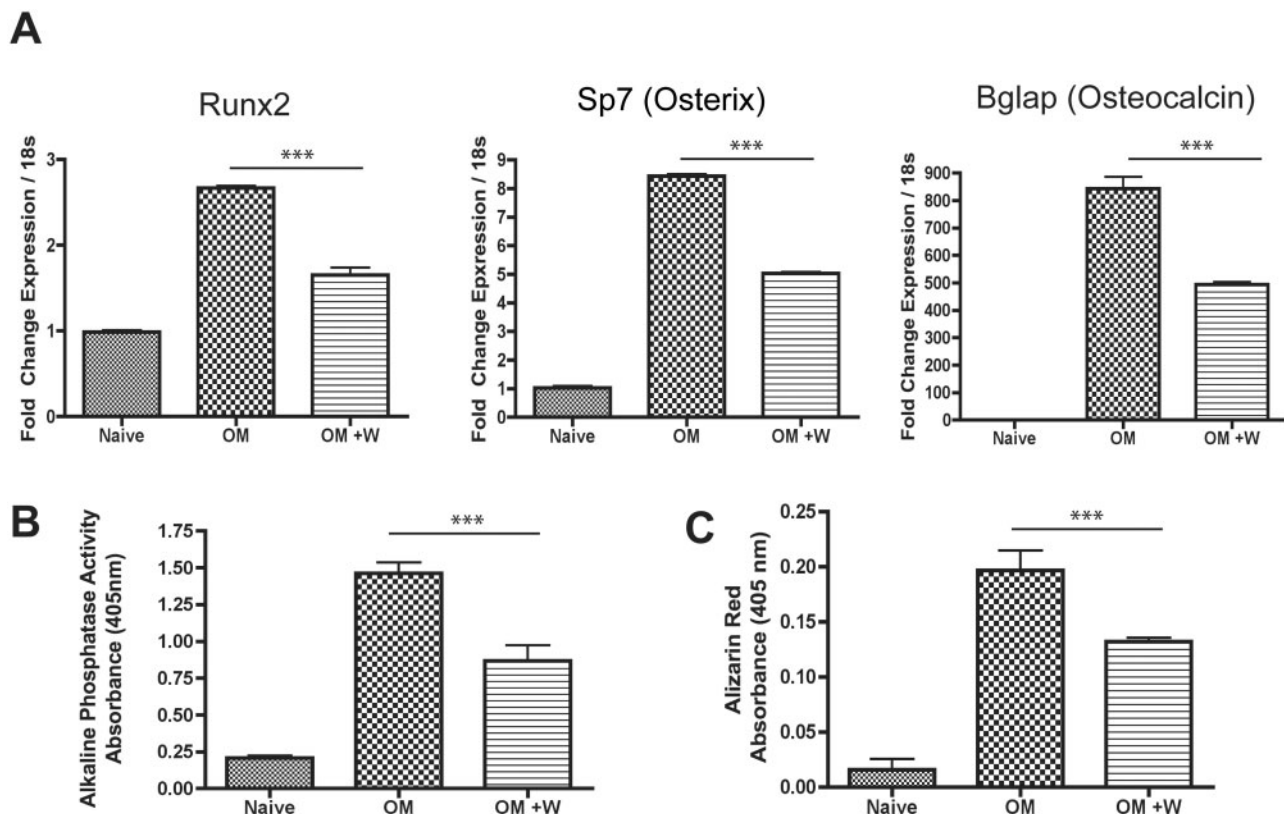
FIG. 3. Tungsten inhibits osteogenesis of MSCs *in vitro*. MSC cultures were transitioned to OM medium and were either left untreated (OM) or treated with 15 μg/ml tungsten (OM +W) throughout osteoblast differentiation. **A,** RNA expression analysis of osteoblast gene markers (*Runx2*, *Sp7*, and *Bglap*) were analyzed by qRT-PCR at day 10 of differentiation. Graph shows the mean fold change in gene expression ± SEM, normalized to naïve gene expression for each gene. Data normalized to housekeeping gene *Rn18s*. ***P ≤ .001 1-way ANOVA. Graph is a representative experiment of 3 biological replicates each performed in four technical replicates. **B,** ALP activity was measured in MSC cultures on day 12 of differentiation. Graph shows the mean level of ALP activity (absorbance) ± SEM for naïve, OM, and OM +W samples. ***P ≤ .001 1-way ANOVA. Graph is a representative experiment of 3 biological replicates each performed in triplicate. **C,** Calcium mineralization was measured by Alizarin Red staining in MSC cultures at day 12 of differentiation. Graph shows the mean level of Alizarin Red dye (absorbance) ± SEM for naïve, OM, and OM +W samples. Graph is a representative experiment of 3 biological replicates each performed in triplicate. ***P ≤ .001 1-way ANOVA.

adipocyte markers. However, Tungsten MSC cultures treated with rosiglitazone had significantly more adipocytes in comparison to rosiglitazone-treated control MSC cultures (Figure 2D). Importantly, these gene expression and phenotypic changes were observed in the absence of tungsten in the culture media. These data further suggest that tungsten exposure is priming MSC cells towards a proadipogenic program and tipping the balance of MSC differentiation.

Tungsten Inhibits Osteogenesis of MSCs *In Vitro*

Promoting adipocyte differentiation of MSCs typically leads to a corresponding inhibition of osteoblast differentiation (Beier *et al.*, 2013; Lecka-Czernik *et al.*, 1999, 2002). Given that tungsten enhances MSC differentiation into adipocytes, we also evaluated the effect of tungsten on MSC differentiation into osteoblasts *in vitro*. MSCs were exposed to OM medium to promote osteogenesis, and when indicated, 15 μg/ml tungsten was added throughout osteoblast differentiation. We evaluated gene expression of osteoblast gene markers by qRT-PCR. Runx2 is the master regulator of osteogenesis and controls the expression of osterix (*Sp7*), which also is an essential osteogenic transcription factor. Osteocalcin (bone gamma-carboxyglutamate protein, *Bglap*) is expressed by late osteoblasts and is involved in mineralization (Bonewald, 2011). On differentiation day 10, tungsten decreased the induction of osteoblast gene markers *Runx2*, *Sp7*,

and *Bglap* compared with the MSCs treated with OM medium alone (Figure 3A). We confirmed that these decreases in gene expression were not due to tungsten-induced apoptosis by evaluating caspase 3/7 activity in MSC cultures (Supplemental Figure S2). Indeed, while staurosporine induced significant cell death within 18 h, no increase in caspase activity was observed with tungsten exposure, even after 10 days of culture. In order to determine whether the decrease in osteogenic gene expression following tungsten exposure had functional consequences, we utilized phenotypic assays of bone formation. ALP activity, an enzyme expressed by osteoblasts, was measured to assess differentiation toward these bone-forming cells. In addition, we measured the amount of mineralization using Alizarin Red staining. Tungsten decreased both ALP activity and Alizarin Red staining (Figs. 3B and C), confirming the gene expression data and suggesting that tungsten decreases osteoblastogenesis. However, it has been reported that high levels of tungsten can directly inhibit phosphatase activity (Foster *et al.*, 1998; Johnson *et al.*, 2010). Therefore, we tested whether 15 μg/ml tungsten directly inhibited ALP activity by adding tungsten to the reaction substrate, instead of culturing the cells in tungsten throughout differentiation. We found no direct inhibition of enzymatic activity by tungsten (Supplemental Figure S3), further supporting the conclusion that tungsten inhibits MSC differentiation into osteoblasts, resulting in a reduction in the amount of bone mineralization *in vitro*.

Tungsten Does Not Inhibit Osteogenesis *In Vivo* after the 4-Week Exposure

Based on these *in vitro* observations, we also evaluated whether tungsten could inhibit osteogenesis *in vivo*. We measured osteoblast gene markers by qRT-PCR in total bone marrow harvested from the mice exposed to 15 ppm tungsten for 4 weeks *in vivo*. We observed no changes in the gene expression levels of osteoblast markers *Runx2*, *Bglap*, and *Sp7* in total bone marrow after the 4-week exposure (Figure 4A). In addition, we evaluated osteoblast content in the bone by detecting ALP activity in tibia bone sections from mice exposed to tungsten *in vivo*. We quantified the amount of ALP in both cortical and trabecular bone regions. Consistent with our total bone marrow RNA analysis, we did not observe any differences in ALP activity in the cortical or trabecular bone regions between control and tungsten-exposed animals (Figure 4B).

Finally, we evaluated osteoblast differentiation of MSCs isolated from control or tungsten-exposed mice and differentiated *in vitro*. After 10 days of differentiation, we measured gene expression of osteoblast gene markers by qRT-PCR. Unlike the *in vitro* treated MSC cultures, we found that tungsten did not decrease the expression of osteoblast markers *Runx2*, *Sp7*, and *Bglap* in MSC cultures from mice exposed to tungsten *in vivo*. We also measured levels of ALP activity and Alizarin Red staining in the cultures at day 12 of differentiation. Consistent with our gene expression results, we found that there were no changes in ALP activity or Alizarin Red staining. These data suggest that a 4-week *in vivo* tungsten exposure does not prime MSCs to be less osteogenic *in vitro*. Thus, contrary to what we observed *in vitro*, tungsten does not alter osteoblast content in the bones of mice after 4 weeks of exposure, despite promoting adipogenesis.

Tungsten-Enhanced Adipogenesis Differs by Sex and Age

The extent of adipogenesis within the bone marrow cavity is regulated by multiple factors, including sex and age. Female mice have lower bone volume and higher adipocyte content than aged-matched male mice (Bragdon *et al.*, 2014). In addition, aging tips the balance of MSC differentiation to favor adipogenesis, while at the same time decreasing osteogenesis (Movahedi *et al.*, 2008). To determine whether tungsten-enhanced adipogenesis was influenced by these factors, we extended our study and exposed young female mice (5 weeks) and adult male and female mice (9 months) to 15 ppm tungsten for 4 weeks. We quantified tungsten concentration and adipocyte content in the bones from control and tungsten-exposed animals for each group. Tungsten concentrations in the humeri bones were not statistically different between young male and female mice, [5.67 ppm ± SEM 1.3 and 4.57 ppm ± SEM 0.46, respectively (Figure 5A)]. However, tungsten concentrations in the bone were affected by age. Adult male mice had no detectable levels of tungsten (< 0.5 ppm, below the limit of detection), while adult female mice had minimal levels of tungsten detected (Figure 5A). In adult females, 3 out of the 4 samples were above the limit of detection (0.61 ppm ± SEM 0.06). This is in stark contrast to the extent of tungsten deposition in the bone that was observed in young mice. These data suggest that changes in bone remodeling that occur with age could be a contributing factor to how tungsten is incorporated into the bone. As previously reported (Bragdon *et al.*, 2014), young female mice had more adipocytes than young male mice, which resulted in a larger area of the bone marrow compartment occupied by adipocytes (Figure 5B). Surprisingly, unlike in the young male mice, tungsten exposure did not enhance adipocyte content in the bone marrow of young female mice (Figure 5B). Adult and young male mice had comparable numbers of adipocytes, but the adipocytes were larger in size in the adult male mice (Figure 5B). However, tungsten did not enhance adipocyte content in adult male mice. The adult female mice had substantially more adipocytes than any other group. Interestingly, after tungsten exposure we observed an increase in the number of adipocytes in the bone (unpaired student *t* test, P = .07) of adult female mice, which resulted in a larger area of the bone occupied by adipocytes (unpaired student *t* test, P = .06). These data suggest that factors, such as age and sex known to enhance adipogenesis, can influence tungsten deposition in the bone and adipogenesis in this model and are important factors to consider when evaluating tungsten-associated toxicities.

DISCUSSION

Tungsten has been highlighted as an emerging contaminant, and yet there is limited knowledge of the potential human health risks. In mice, tungsten accumulates in the bone and provides a source of long-term exposure, even if the external exposure is removed (Kelly *et al.*, 2013). Here, we demonstrate that tungsten deposition in the bone has a significant impact on bone homeostasis.

We found that *in vivo*, tungsten promotes adipocyte differentiation in young male mice and *in vitro*, stimulates rosiglitazone-induced adipogenesis. Interestingly, a growing list of agents including thiazolidinediones (rosiglitazone), organotins, organophosphate flame retardants, and phthalates promote adipogenesis of MSCs, in part, through acting as a ligand for PPARγ (Feige *et al.*, 2007; Gimble *et al.*, 1996; Pillai *et al.*, 2014; Watt *et al.*, 2015; Yanik *et al.*, 2011). However, tungsten does not promote adipogenesis through the same mechanism. Tungsten did not activate the PPARγ-driven response element, and tungsten alone did not induce adipogenesis in bone marrow MSCs. However, tungsten significantly enhanced rosiglitazone (PPARγ ligand)-induced gene expression and adipogenesis, suggesting that tungsten may enhance adipogenesis by promoting the PPARγ ligand-induced programming. Indeed, *in vivo* tungsten exposure increased *ex vivo* adipogenesis alone and in combination with rosiglitazone. These data suggest that tungsten could be enhancing adipogenesis by reprograming MSCs to be proadipogenic and tipping the balance of MSC differentiation toward adipogenesis. Tungsten could act upstream of PPARγ by enhancing expression or function of CCAAT/Enhancer Binding Proteins (C/EBP) C/EBPβ, C/EBPδ, and C/EBPα or members of the Mitogen-Activating Protein Kinase Kinase (MEK)/Extracellular Signaling-Regulated Kinases (ERK) signaling pathway known to be co-factors for PPARγ signaling that lead to adipogenesis (Clarke *et al.*, 1997; Moldes *et al.*, 2003; Prusty *et al.*, 2002; Salma *et al.*, 2006). Alternatively, tungsten may support adipogenesis by interacting with the Wnt/β-catenin signaling pathway (Day *et al.*, 2005). Inhibition of the Wnt/β-catenin signaling pathway can promote adipogenesis through induction of C/EBPβ and PPARγ (Moldes *et al.*, 2003). Further experiments are needed to dissect the mechanisms of tungsten-altered MSC differentiation leading to enhanced adipogenesis.

Although tungsten suppressed osteogenic gene expression and bone deposition *in vitro*, we did not observe a decrease in osteogenesis *in vivo*. This suggests that tungsten has more profound effects on adipogenesis than bone formation, but it is also possible that a 4-week exposure is not the optimal
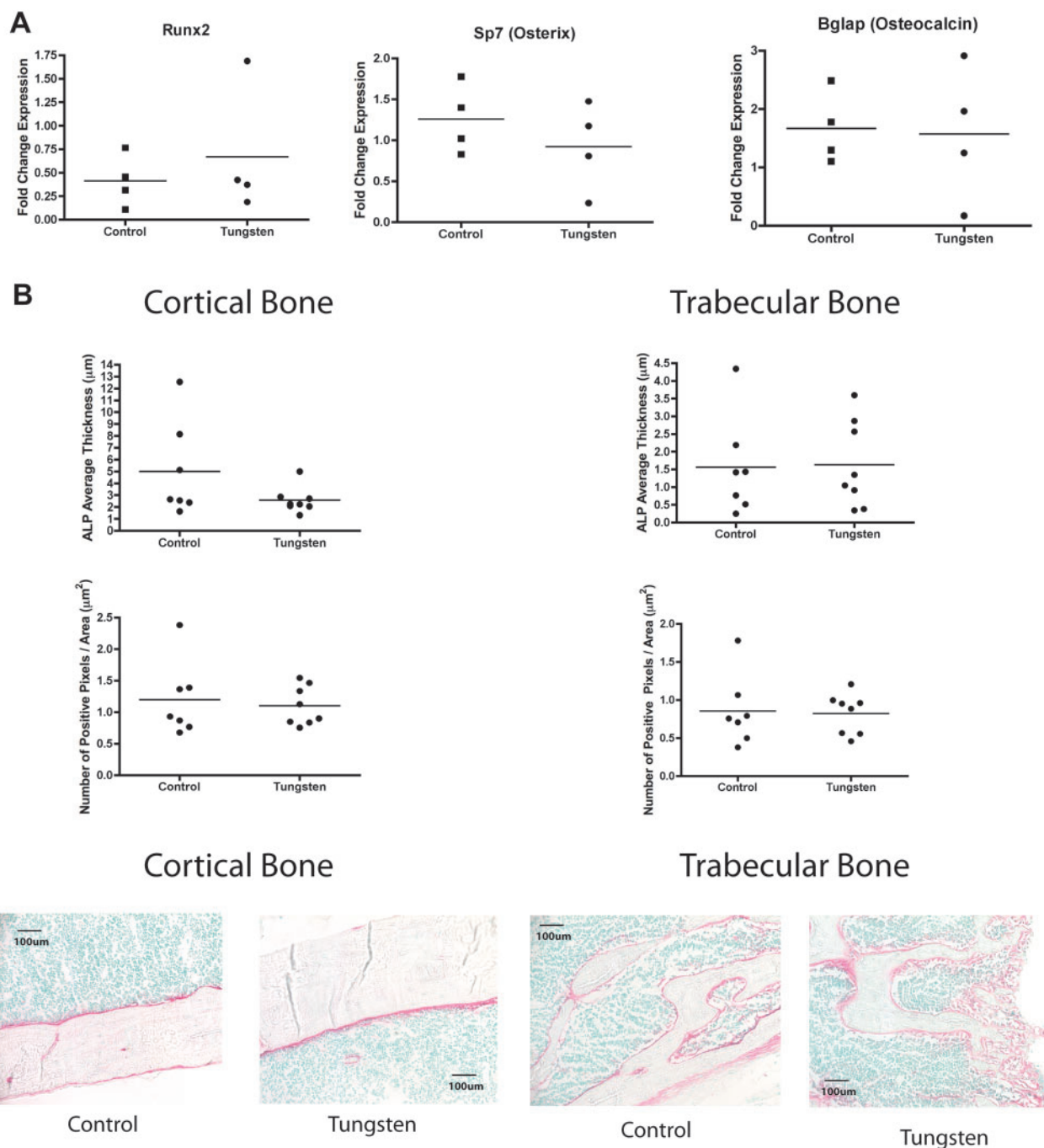
FIG. 4. Tungsten does not inhibit osteogenesis *in vivo* **A,** RNA expression analysis of osteogenic gene markers *Runx2*, *Sp7*, and *Bglap* in total bone marrow isolated from control and tungsten-exposed animals, analyzed by qRT-PCR. Graph shows mean fold change in gene expression normalized to one control sample ($n = 4$). Data normalized to housekeeping genes *Gapdh* and *m36B4*. **B,** Analysis of ALP activity in sections of tibia bone tissue from control and tungsten-exposed animals. Graphs show the average ALP staining thickness (μm)/animal and the number of positive pixels/analyzed region area (μm^2)/animal ($n \geq 7$). Representative images of ALP staining in cortical (left) and trabecular (right) bone regions from control and tungsten-exposed tibia sections, 20×. **C,** *Ex vivo* cultures were isolated from control and tungsten-exposed mice and differentiated in the absence of tungsten *in vitro*. MSC cultures were transitioned to OM medium throughout differentiation (Control OM or Tungsten OM). RNA expression analysis of osteogenic gene markers (*Runx2*, *Sp7*, and *Bglap*) in *ex vivo* MSC cultures analyzed by qRT-PCR at day 10 of differentiation. Graph shows the mean fold change in gene expression ± SEM ($n = 3$), normalized to naïve gene expression for each gene. **D,** ALP activity was measured in *ex vivo* MSC cultures on day 12 of differentiation. Graph shows the mean level of ALP activity (absorbance) ± SEM for naïve, Control OM, and Tungsten OM samples ($n = 6$). **E,** Calcium mineralization was measured by Alizarin Red staining in *ex vivo* MSC cultures at day 12 of differentiation. Graph shows the mean level of Alizarin Red dye (absorbance) ± SEM for naïve, Control OM, and Tungsten OM samples ($n = 6$).

exposure time at which to evaluate changes in osteoblast activity in the bone marrow. The changes induced by tungsten at 4 weeks may be subtle given the relatively short exposure duration. In rats exposed to lead, researchers observed decreases in expression of osteoblast gene markers and the number of osteoblasts present in the bone marrow after being exposed throughout their lifetime (18 months) (Beier *et al.*, 2013). In addition, in bone sections from arsenic-exposed rats, researchers observed
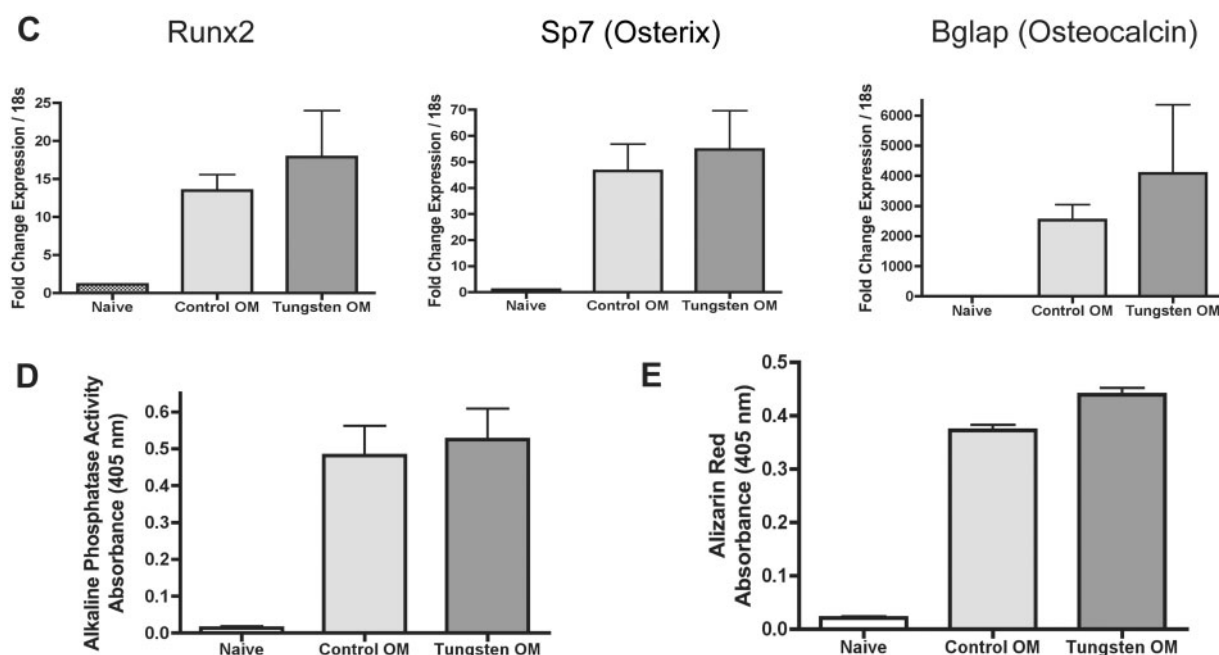
FIG. 4. Continued

decreases in Runx2 expression at 12 weeks of exposure (Wu et al., 2014). We also observed that tungsten-inhibition of osteo-genesis required longer than tungsten-enhanced adipogenesis in the MSC cultures (7 vs 10 days), which could further suggest that in order to observe tungsten's effects on osteoblast differ-entiation *in vivo*, longer exposures would be required. Additionally, we have focused on osteoblast number (ALP) and mineralization (Alazirin Red) at one time point. However, the bone is a dynamic organ that is constantly remodeling. Bone re-modeling is a tightly controlled process consisting of the bal-ance between bone formation, regulated by osteoblasts and bone resorption, regulated by osteoclasts. In order to have a more comprehensive picture of how tungsten affects bone biol-ogy, we are currently evaluating the effects of tungsten on bone resorption by determining the effects of tungsten on osteoclast differentiation and function as this information will provide in-sight into how tungsten affects overall bone remodeling.

Of note, we observed that tungsten bone concentrations and effects on adipogenesis varied with both sex and age. Even though young male and female mice had comparable tungsten burden in the bone, tungsten increased adipogenesis only in the males. Young, female mice had more adipocytes at a basal level, but tungsten did not further enhance adipogenesis. One explan-ation for this difference is that hormones in the female mice are masking the effect of tungsten on adipogenesis. Researchers have found that in intact female rats, rosiglitazone did not change bone mass or fat marrow mass, but observed enhanced bone loss and increased fat marrow content in ovariectomized females (Sottile et al., 2004). Surprisingly, we found that older mice had dramatically less tungsten accumulated in the bone than younger mice. This may be explained by the decreased rate of bone formation or growth associated with aging. Throughout the aging process, bone growth stops and the rate and extent of bone remodeling changes, which could potentially affect how tungsten accumulates in the bone. (Reviewed in Boskey and Coleman, 2010). We have also observed that in a mouse model of breast cancer, tungsten deposition in the bone

was 2 times higher in tumor-bearing than in non-tumor bearing mice (Bolt et al., 2015). Altered bone remodeling is a common characteristic of cancer, particularly in cancers that are known to metastasize to the bone (Grano et al., 2000) and could be an explanation for the altered tungsten deposition in the bone observed. Interestingly, we observed that tungsten increased adipocyte number and area within the bone marrow in adult fe-male mice, even in the absence of substantial bone accumula-tion. This could indicate that even low levels of bone tungsten could have effects in older females. Alternatively, altered adipo-genesis in older females may be through a different tungsten-induced mechanism, independent of bone deposition. These data further highlight the importance of evaluating the influ-ence of altered bone remodeling on tungsten deposition in the bone, particularly as it may help to identify susceptible win-dows of exposure.

Together, our data identify bone as a new target of tungsten toxicity and provide evidence that tungsten deposition in the bone may have an impact on bone health. Similar changes in MSC differentiation induced by lead and rosiglitazone correlate with significantly decreased bone mineral density and bone strength indicative of osteoporosis (Beier et al., 2013; Lazarenko et al., 2007). Furthermore, bone marrow-resident MSCs contribute to more than just bone integrity, but also regulate hematopoiesis. Adipocyte-rich bone marrow suppresses hem-atopoiesis, whereas osteoblasts supporting hematopoiesis (Calvi et al., 2003; Naveiras et al., 2009). One could hypothesize that altering the balance of MSC differentiation in the bone to promote adipogenesis would have a negative impact on hem-atopoietic development and potentially, immune responses. Interestingly, mice exposed to tungsten exhibit altered B lymphocyte differentiation (Kelly et al., 2013), increased Gr1+ myeloid-derived suppressor cells in response to tumor (Bolt et al., 2015), and an altered anti-viral immune response (Fastje et al., 2012). Thus, tungsten may have effects on more than just bone, further justifying it's placement on the National Toxicology Program Priority Substance List (NTP, 2002).
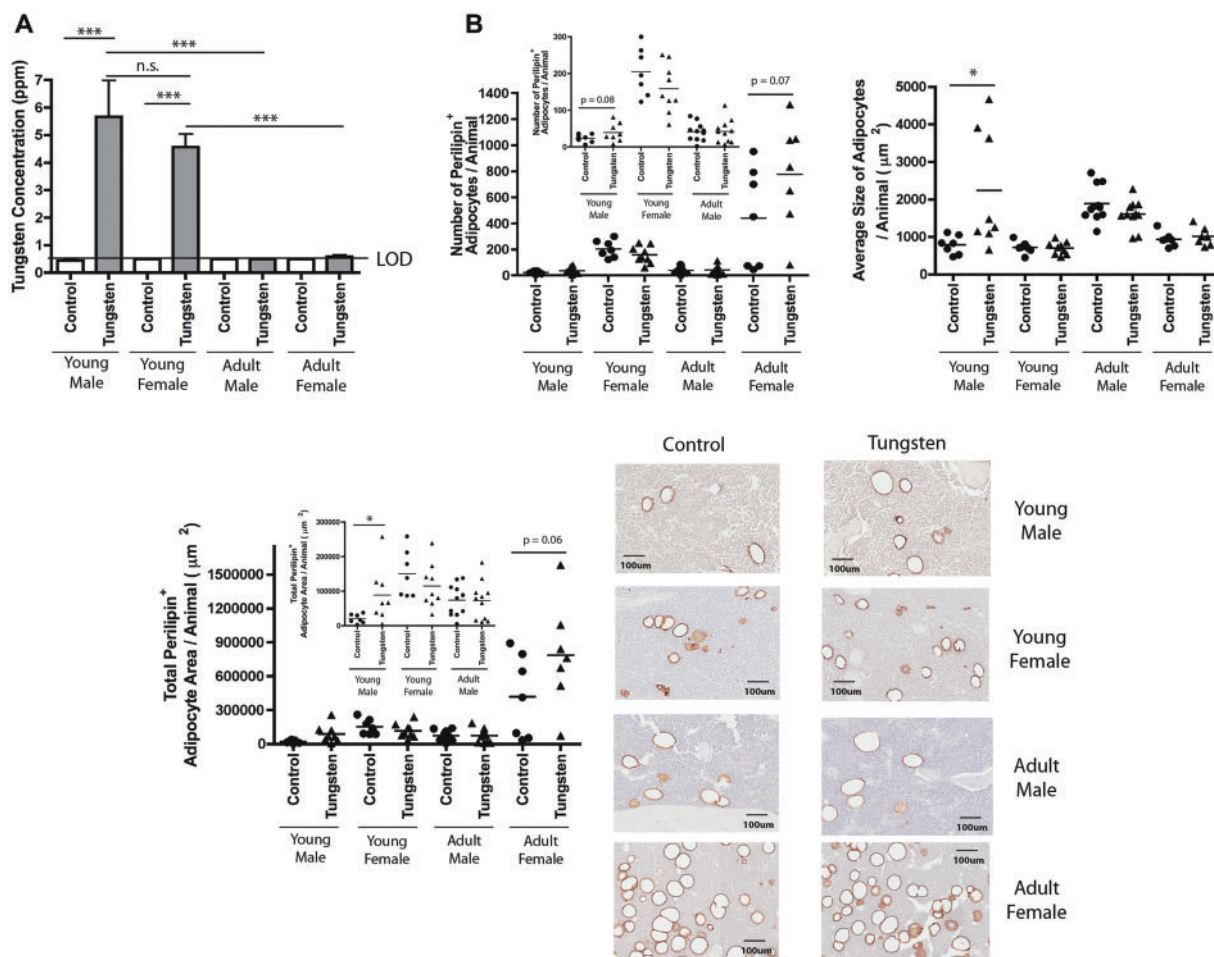
FIG. 5. Tungsten-enhanced adipogenesis is influenced by sex and age of mice. **A,** Tungsten concentration in humeri bones measured by ICP-MS. Graph shows the mean ± SEM tungsten concentration in humeri bones in young (5 weeks) male and female, and adult (9 months) male and female mice, given tap water or 15 ppm in drinking water for 4 weeks ($n \geq 4$). ***$P \leq .001$ 1-way ANOVA. **B,** Analysis of perilipin staining by IHC in sections of femur bone tissue from control and tungsten-exposed animals (young male and female; middle-aged male and female mice). Graphs show the mean number of perilipin[+] adipocytes/animal, average size of each adipocyte/animal, and the total perilipin[+] adipocyte area/animal ($n \geq 7$). Representative images of perilipin[+] adipocytes in control and tungsten-exposed femur sections, 20×. *$P \leq .05$ unpaired student t test, 1-tailed comparisons between control and tungsten-exposed animals per group.

SUPPLEMENTARY DATA

Supplementary data are available online at http://toxsci. oxfordjournals.org/.

FUNDING

REFERENCES

Bachthaler, M., Lenhart, M., Paetzel, C., Feuerbach, S., Link, J., and Manke, C. (2004). Corrosion of tungsten coils after peripheral vascular embolization therapy: Influence on outcome and tungsten load. *Catheter. Cardiovasc. Interv.* **62**, 380–384.

Beier, E. E., Maher, J. R., Sheu, T. J., Cory-Slechta, D. A., Berger, A. J., Zuscik, M. J., and Puzas, J. E. (2013). Heavy metal lead exposure, osteoporotic-like phenotype in an animal model, and depression of Wnt signaling. *Environ. Health Perspect.* **121**, 97–104.

Bolt, A. M., Sabourin, V., Molina, M. F., Police, A. M., Negro Silva, L. F., Plourde, D., Lemaire, M., Ursini-Siegel, J., and Mann, K. K. (2015). Tungsten targets the tumor microenvironment to enhance breast cancer metastasis. *Toxicol. Sci.* **143**, 165–177.

Bonewald, L. F. (2011). The amazing osteocyte. *J. Bone Miner. Res.* **26**, 229–238.

Boskey, A. L., and Coleman, R. (2010). Aging and bone. *J. Dent. Res.* **89**, 1333–1348.

Bragdon, B., Burns, R., Baker, A. H., Belkina, A. C., Morgan, E. F., Denis, G. V., Gerstenfeld, L. C., and Schlezinger, J. J. (2014). Intrinsic sex-linked variations in osteogenic and adipogenic differentiation potential of bone marrow multipotent stromal cells. *J. Cell Physiol.* **230**(2), 296–307.

Calvi, L. M., Adams, G. B., Weibrecht, K. W., Weber, J. M., Olson, D. P., Knight, M. C., Martin, R. P., Schipani, E., Divieti, P., Bringhurst, F. R., *et al.*, (2003). Osteoblastic cells regulate the haematopoietic stem cell niche. *Nature* **425**, 841–846.

Cheng, H., Qiu, L., Zhang, H., Cheng, M., Li, W., Zhao, X., Liu, K., Lei, L., and Ma, J. (2011). Arsenic trioxide promotes senescence and regulates the balance of adipogenic and osteogenic differentiation in human mesenchymal stem cells. *Acta Bioch. Bioph. Sin.* **43**, 204–209.

Clarke, S. L., Robinson, C. E., and Gimble, J. M. (1997). CAAT/enhancer binding proteins directly modulate transcription from the peroxisome proliferator-activated receptor gamma 2 promoter. *Biochem. Bioph. Res. Co.* **240**, 99–103.

Day, T. F., Guo, X., Garrett-Beal, L., and Yang, Y. (2005). Wnt/beta-catenin signaling in mesenchymal progenitors controls osteoblast and chondrocyte differentiation during vertebrate skeletogenesis. *Dev. Cell* **8**, 739–750.

EPA. (2008). Emerging contaminant tungsten. Fact sheet. 505-F-07-005. Available at: http://www.epa.gov/nscep. Accessed October 15, 2015.

EPA. (2012). Technical Fact Sheet-Tungsten. 505-F-11-005. Available at: http://www.epa.gov/nscep. Accessed October 15, 2015.

Fastje, C. D., Harper, K., Terry, C., Sheppard, P. R., and Witten, M. L. (2012). Exposure to sodium tungstate and Respiratory Syncytial Virus results in hematological/immunological disease in C57BL/6J mice. *Chem-Biolo. Interact.* **196**, 89–95.

Feige, J. N., Gelman, L., Rossi, D., Zoete, V., Metivier, R., Tudor, C., Anghel, S. I., Grosdidier, A., Lathion, C., Engelborghs, Y., *et al.* (2007). The endocrine disruptor monoethyl-hexyl-phthalate is a selective peroxisome proliferator-activated receptor gamma modulator that promotes adipogenesis. *J. Biol. Chem.* **282**, 19152–19166.

Foster, J. D., Young, S. E., Brandt, T. D., and Nordlie, R. C. (1998). Tungstate: A potent inhibitor of multifunctional glucose-6-phosphatase. *Arch. Biochem. Biophs.* **354**, 125–132.

Gimble, J. M., Robinson, C. E., Wu, X., Kelly, K. A., Rodriguez, B. R., Kliewer, S. A., Lehmann, J. M., and Morris, D. C. (1996). Peroxisome proliferator-activated receptor-gamma activation by thiazolidinediones induces adipogenesis in bone marrow stromal cells. *Mol. Pharmacol.* **50**, 1087–1094.

Grano, M., Mori, G., Minielli, V., Cantatore, F. P., Colucci, S., and Zallone, A. Z. (2000). Breast cancer cell line MDA-231 stimulates osteoclastogenesis and bone resorption in human osteoclasts. *Biochem. Bioph. Res. Co.* **270**, 1097–1100.

Greenberg, A. S., Egan, J. J., Wek, S. A., Garty, N. B., Blanchette-Mackie, E. J., and Londos, C. (1991). Perilipin, a major hormonally regulated adipocyte-specific phosphoprotein associated with the periphery of lipid storage droplets. *J. Biol. Chem.* **266**, 11341–11346.

Guandalini, G. S., Zhang, L., Fornero, E., Centeno, J. A., Mokashi, V. P., Ortiz, P. A., Stockelman, M. D., Osterburg, A. R., and Chapman, G. G. (2011). Tissue distribution of tungsten in mice following oral exposure to sodium tungstate. *Chem. Res. Toxicol.* **24**, 488–493.

Johnson, D. R., Ang, C., Bednar, A. J., and Inouye, L. S. (2010). Tungsten effects on phosphate-dependent biochemical pathways are species and liver cell line dependent. *Toxicol. Sci.* **116**, 523–532.

Kelly, A. D., Lemaire, M., Young, Y. K., Eustache, J. H., Guilbert, C., Flores Molina, M., and Mann, K. K. (2013). in vivo tungsten exposure alters B cell development and increases DNA damage in murine bone marrow. *Toxicol. Sci.* **131**, 434–446.

Klei, L. R., Garciafigueroa, D. Y., and Barchowsky, A. (2013). Arsenic activates endothelin-1 Gi protein-coupled receptor signaling to inhibit stem cell differentiation in adipogenesis. *Toxicol. Sci.* **131**, 512–520.

Lazarenko, O. P., Rzonca, S. O., Hogue, W. R., Swain, F. L., Suva, L. J., and Lecka-Czernik, B. (2007). Rosiglitazone induces decreases in bone mass and strength that are reminiscent of aged bone. *Endocrinology* **148**, 2669–2680.

Lecka-Czernik, B., Gubrij, I., Moerman, E. J., Kajkenova, O., Lipschitz, D. A., Manolagas, S. C., and Jilka, R. L. (1999). Inhibition of Osf2/Cbfa1 expression and terminal osteoblast differentiation by PPARgamma2. *J. Cell Biochem.* **74**, 357–371.

Lecka-Czernik, B., Moerman, E. J., Grant, D. F., Lehmann, J. M., Manolagas, S. C., and Jilka, R. L. (2002). Divergent effects of selective peroxisome proliferator-activated receptor-gamma 2 ligands on adipocyte versus osteoblast differentiation. *Endocrinology* **143**, 2376–2384.

Mann, K. K., Padovani, A. M., Guo, Q., Colosimo, A. L., Lee, H. Y., Kurie, J. M., and Miller, W. H. Jr. (2005). Arsenic trioxide inhibits nuclear receptor function via SEK1/JNK-mediated RXRalpha phosphorylation. *J. Clin. Invest.* **115**, 2924–2933.

Moldes, M., Zuo, Y., Morrison, R. F., Silva, D., Park, B. H., Liu, J., and Farmer, S. R. (2003). Peroxisome-proliferator-activated receptor gamma suppresses Wnt/beta-catenin signalling during adipogenesis. *Biochem. J.* **376(Pt 3)**, 607–613.

Movahedi, K., Guilliams, M., Van den Bossche, J., Van den Bergh, R., Gysemans, C., Beschin, A., De Baetselier, P., and Van Ginderachter, J. A. (2008). Identification of discrete tumor-induced myeloid-derived suppressor cell subpopulations with distinct T cell-suppressive activity. *Blood* **111**, 4233–4244.

Naveiras, O., Nardi, V., Wenzel, P. L., Hauschka, P. V., Fahey, F., and Daley, G. Q. (2009). Bone-marrow adipocytes as negative regulators of the haematopoietic microenvironment. *Nature* **460**, 259–263.

NIOSH. (1977). Occupational exposure to tungsten and cemented carbide. 21–171. Available at: http://www.cdc.gov/niosh/docs/1970/77-227.html. Accessed October 15, 2015.

NTP. (2002). Priority Substance List Nomination Summary - Tungsten. Available at: http://ntp.niehs.nih.gov/testing/noms/search/summary/nm-n20226.html. Accessed October 15, 2015.

Park, B. H., Qiang, L., and Farmer, S. R. (2004). Phosphorylation of C/EBPbeta at a consensus extracellular signal-regulated kinase/glycogen synthase kinase 3 site is required for the induction of adiponectin gene expression during the differentiation of mouse fibroblasts into adipocytes. *Mol. Cell Biol.* **24**, 8671–8680.

Pillai, H. K., Fang, M., Beglov, D., Kozakov, D., Vajda, S., Stapleton, H. M., Webster, T. F., and Schlezinger, J. J. (2014). Ligand binding and activation of PPARgamma by Firemaster(R) 550: Effects on adipogenesis and osteogenesis in vitro. *Environ. Health Perspect.* **122**, 1225–1232.

Prusty, D., Park, B. H., Davis, K. E., and Farmer, S. R. (2002). Activation of MEK/ERK signaling promotes adipogenesis by enhancing peroxisome proliferator-activated receptor gamma (PPARgamma) and C/EBPalpha gene expression during the differentiation of 3T3-L1 preadipocytes. *J. Biol. Chem.* **277**, 46226–46232.

Rubin, C. S., Holmes, A. K., Belson, M. G., Jones, R. L., Flanders, W. D., Kieszak, S. M., Osterloh, J., Luber, G. E., Blount, B. C., Barr, D. B., *et al.* (2007). Investigating childhood leukemia in Churchill County, Nevada. *Environ. Health Perspect.* **115**, 151–157.

Salma, N., Xiao, H., and Imbalzano, A. N. (2006). Temporal recruitment of CCAAT/enhancer-binding proteins to early and late adipogenic promoters in vivo. *J. Mol. Endocrinol.* **36**, 139–151.

Sottile, V., Seuwen, K., and Kneissel, M. (2004). Enhanced marrow adipogenesis and bone resorption in estrogen-deprived rats treated with the PPARgamma agonist BRL49653 (rosiglitazone). *Calcified Tissue Int.* **75**, 329–337.

Tontonoz, P., Hu, E., Graves, R. A., Budavari, A. I., and Spiegelman, B. M. (1994). mPPAR gamma 2: Tissue-specific regulator of an adipocyte enhancer. *Gen. Dev.* **8**, 1224–1234.

Tyrrell, J., Galloway, T. S., Abo-Zaid, G., Melzer, D., Depledge, M. H., and Osborne, N. J. (2013). High urinary tungsten concentration is associated with stroke in the National Health and Nutrition Examination Survey 1999-2010. *PloS One* **8**, e77546.

Watt, J., and Schlezinger, J. J. (2015). Structurally-diverse, PPARgamma-activating environmental toxicants induce adipogenesis and suppress osteogenesis in bone marrow mesenchymal stromal cells. *Toxicology* **331**, 66–77.

Wu, C. T., Lu, T. Y., Chan, D. C., Tsai, K. S., Yang, R. S., and Liu, S. H. (2014). Effects of arsenic on osteoblast differentiation in vitro and on bone mineral density and microstructure in rats. *Environ. Health Perspect.* **122**, 559–565.

Yanik, S. C., Baker, A. H., Mann, K. K., and Schlezinger, J. J. (2011). Organotins are potent activators of PPARgamma and adipocyte differentiation in bone marrow multipotent mesenchymal stromal cells. *Toxicol. Sci.* **122**, 476–488.